

Mass Transport and Potential Studies in a Flow-Through Porous Electrode Reactor. Effect of the Carbon Particle Size, Used as a Porous Cathode, During the Deposition of Silver Ions

José L. Nava^{1,*}, Mercedes T. Oropeza², Gilberto Carreño¹

¹Universidad de Guanajuato, Departamento de Ingeniería Geomática e Hidráulica, Av. Juárez No. 77, C.P. 36000, Guanajuato, Guanajuato, México.

²Instituto Tecnológico de Tijuana, Centro de Graduados e Investigación, Blvd. Industrial s/n, CP 22500, Tijuana, B. C., México.

*E-mail: jlnm@ugto.mx

Received: 12 May 2013 / Accepted: 28 July 2013 / Published: 10 September 2013

The mass transport and potential characterization were carried out in a flow-through porous electrode reactor. Carbon particles of three different sizes were used as porous electrode. Silver electrodeposition from an alkaline ammonia electrolyte is used as a test system. The experimental mass transport characterization ($k_m a = bu^c$) showed that the value of the coefficient b depends on the magnitude of carbon particle, while c indicates that the flow pattern is a complex function of the carbon particle size. The experimental potential drop in the flow-through porous electrode is also reported. The mass transport and potential characterization have been conducted to identify suitable operating conditions.

Keywords: Silver electrodeposition, Flow-through porous electrode reactor, Mass transport characterization, Potential distribution.

1. INTRODUCTION

Packed bed electrodes can be used for electrochemical recovery of heavy metals from a variety of industrial and laboratory model solutions [1-12]. The packed bed electrode forms a porous flow-through configuration providing large surface area usually depleting the concentration of metal ions below 0.1 ppm.

Several forms of flow-through porous electrodes have been employed for the removal of heavy metals, such as graphite felt (GF) [13], carbon particles [1], zinc spheres [10], silver coated glass [14],

platinum screen [15], reticulated vitreous carbon (RVC) [6,16], stainless-steel fibers [7], nickel felts and nickel foams [17], to mention some of them. Experimental mass transport correlations obtained in this kind of flow-through reactors, when electrodes usually work under mass transport control, evidenced disagreement between authors. This last is attributed to the electrode material, shape, electrode area, and reaction mechanism (nature of the new metallic phase) involved [13, 16].

It is well known that during the depletion of the metal ions from the solutions a potential and current distribution along the cathode occurs [1-3, 6, 7, 10-12, 16]. For this reason, it is highly recommendable to design thick porous electrodes with moderate flow rate of electrolyte [1-3, 6, 7, 16] to avoid secondary reactions which impact in the performance of the flow through porous electrode.

The aim of this paper is to characterize the mass transport and potential drop to identify suitable operating conditions of a flow-through porous electrode reactor during a metal recovery process avoiding secondary reactions such as the hydrogen evolution. This is shown by taking the deposition of Ag(I) ions on three carbon particles porous cathodes of different sizes. The potential for the reduction of Ag(I) ions at mass transport controlled conditions was selected for the electrolysis experiments in a flow-through porous electrode.

2. MASS BALANCE IN A RECIRCULATING FLOW-THROUGH REACTOR WITH 3D ELECTRODE

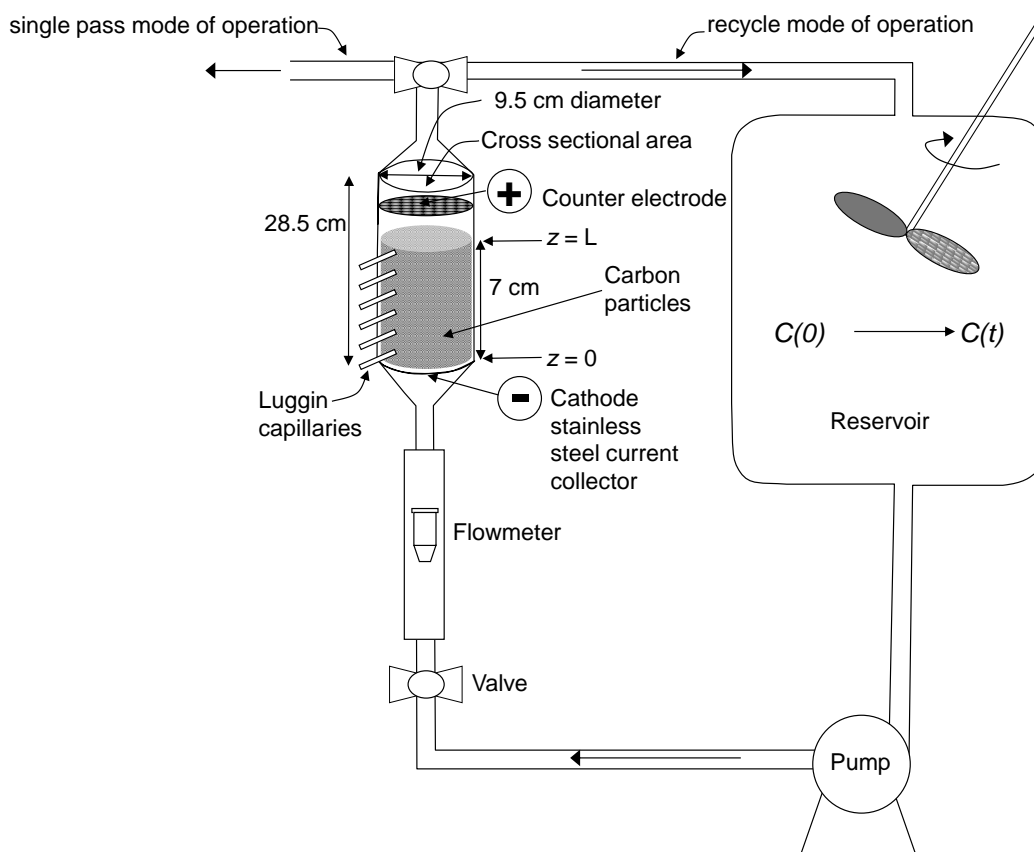


Figure 1. Experimental flow circuit and flow-through porous electrode reactor.

The concentration profile of the electroactive species in a flow-through reactor in batch recycle mode of operation (see Figure 1), neglecting phase changes and dispersion effects in the porous electrode, can be described by the following equation [18]:

$$\frac{C(t)}{C(t=0)} = \exp\left[-\frac{t}{\tau_T} (1 - \exp^{-[\alpha L]})\right] \quad (1)$$

where $C(t)$ and $C(t=0)$ are the concentration of the electroactive species during the electrolysis at time t and 0 respectively, τ_T is the mean residence time of the electrolyte in the reservoir defined as $\tau_T = V_T/Q$, where V_T and Q are the volume of the reservoir and the volumetric flow rate. L is the length of the porous electrode and α is the following group parameter:

$$\alpha = \frac{k_m a (1 - \varepsilon)}{u} \quad (2)$$

where k_m is the average mass transport coefficient assuming that it is independent of the axial position (z), a is the specific surface electrode area (a =electrode area/volume occupied by the whole electrode), ε is the electrode porosity and u is the mean linear flow velocity of the electrolyte.

The equation (1) can be expressed in terms of the fractional removal of the electroactive specie as follows:

$$X = 1 - \exp\left[-\frac{t}{\tau_T} (1 - \exp^{-[\alpha L]})\right] \quad (3)$$

When designing a flow-through porous electrode reactor, it is necessary to know the mass transport rate towards the electrode surface in given hydrodynamic conditions. The mass transport correlations in flow-through porous electrodes can be expressed as equation (4):

$$k_m a = b u^c \quad (4)$$

Where b is a constant associated with shape of the electrode and cell dimensions, and c is a constant associated with hydrodynamics.

3. EXPERIMENTAL

3.1. Equipment and solutions

The electrolyte consisted of $4.6 \times 10^{-3} \text{ mol dm}^{-3}$ AgNO_3 , 0.1 mol dm^{-3} KNO_3 and 0.6 mol dm^{-3} NH_4OH and was prepared using analytical grade reactants dissolved in deionized water (Milli-QTM).

This solution was used for the flow cell experiments. In the flow cell, 5 L of this solution were circulated through the electrolyte circuit (Figure 1).

3.2. Experiments in the packed bed flow cell

Figure 1 shows a schematic diagram of the packed bed flow cell; the body of the reactor consists of a propylene tube of 28.5 cm length and 9.5 cm internal diameter. The tube was fitted with flanges at both ends. Two Nylon cones with a flange were attached at the top and bottom of the tube using the flanges in order to form the inlet and outlet of the reactor. The conical shape improves the distribution of the fluid at the inlet and avoids back mixing of the electrolyte at the exit. The polypropylene tube contained carbon particles as a cathode electrode. Three different carbon particle size supported by a stainless steel mesh current collector of 9.4 cm diameter were used separately as porous electrodes.

Table 1. Porosity of the three carbon particle porous electrodes of 1.91 g cm^{-3} density contained in reactor of 71 cm^2 cross sectional area and 7 cm long.

Particle size* (dp) / cm	Porosity (ϵ)
0.11	0.33
0.24	0.35
0.30	0.36

*The carbon particle size was calculated by multiplication of the sphericity of the particle (0.6, dimensionless) by the corresponding mesh fraction of carbon particle.

Table 1 shows the parameters of carbon particles. Small plastic tubes inserted on 3 mm holes drilled along the propylene tube length were used as Luggin capillaries to monitor the local potential throughout the packed bed electrode (see Figure 1). A titanium mesh covered with a layer of RuO_2 was used as counter electrode at the top of the reactor.

A March MFG pump of 1/25 hp was used to recirculate the electrolyte through the reactor and the flow rates were measured using a variable area polycarbonate flowmeter (Cole Palmer model F44376LH-8). The electrolyte flow circuit was constructed with Master Flex tubing, (C-Flex 6424-16, 0.5 inch diameter). All the valves and three way connectors were assembled with PVC materials. The electrolyte was contained in a 5 L reservoir fitted with a stainless-steel stirrer powered by a 115 V Caframo™ electric motor of variable velocity used to achieve well mixed conditions. The electrolyte circuit was designed to allow single pass or recirculation modes of operation.

During electrolysis, the concentration of silver ions was potentiometrically determined using an ion selective electrode (ISE) model 9616N from Orion Research Inc.™. The electrode was calibrated each time a new sets of samples from a different experiment were taken and was allowed to equilibrate with solutions of similar concentration of Ag(I) ions expected from the samples.

A power supply model PE 1516 from PhillipsTM was used to apply the current of particles porous electrodes. The potential along the porous electrode, $\varphi(z)$, was monitored with a saturated sulfate reference electrode SSE ($E = 615$ mV vs. SHE), connected to the Luggin capillaries and switched to high impedance multimeter model 34401A from AgilentTM. All potentials are referred to the standard hydrogen electrode, SHE. The solutions were deoxygenated during approximately 10 minutes before the tests and the experiments were carried out at 25 ± 1 °C.

4. ANALYSIS OF RESULTS AND DISCUSSION

The mass transport coefficients were determined by electrolysis of Ag(I) ion solutions in the packed bed flow-through reactor in recycle mode of operation (Figure 1). The electrolysis were performed by applying a potential on the current collector, at $z = 0$, $\varphi(z=0) = 0.7$ V vs. SHE, situated at the inlet of the packed bed electrode reactor. At such potential the cathodic process, in the carbon particles used as porous electrode, is mass transport controlled. The mean linear flow velocities during the electrolysis were between 0.24 and 0.94 cm s⁻¹.

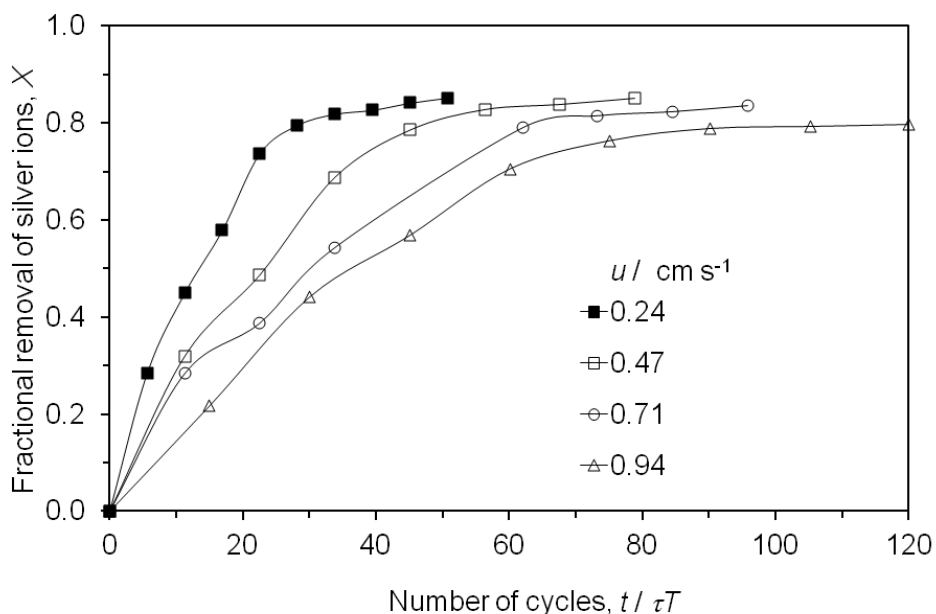


Figure 2. Fractional removal of silver ions vs. number of cycles. Carbon particle size of 0.11 cm. Electrolysis potential $\varphi(z=0) = -0.7$ V vs. SHE. Mean linear flow electrolyte velocities are showed inside the Figure.

Figure 2 shows the fractional removal of silver ions, X , as a function of the number of cycles, $t/\tau T$, at different mean linear flow velocities for a size of carbon particle of 0.11 cm. The fractional removal of silver ions requires more number of cycles as mean linear flow velocity increases. Based on

the curves shown in Figure 2, the values of mass transport coefficients were obtained applying the equation (3).

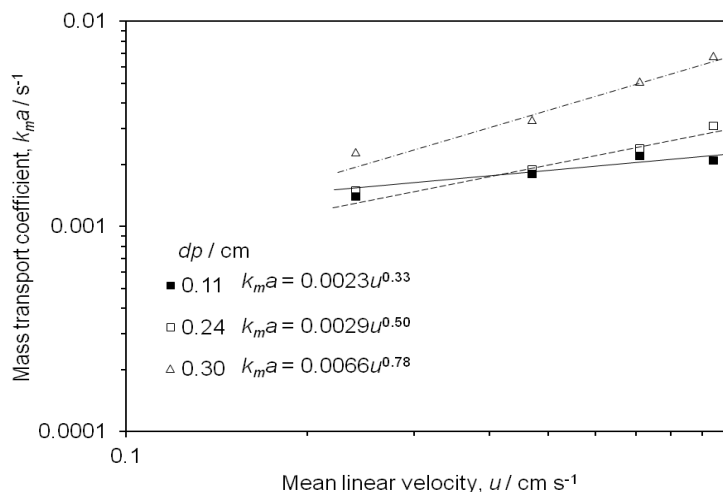


Figure 3. Mass transport coefficients vs. mean linear flow electrolyte velocity for the reduction of Ag(I) ions. Carbon particles sizes are showed inside the figure.

Figure 3 shows the mean mass transport coefficients multiplied by the specific surface electrode area vs. mean linear flow electrolyte velocity ($k_m a$ vs. u), for the three carbon particle sizes. The mass transport coefficients increased with the particle size of each electrode and with the mean linear flow velocity of the electrolyte; this last is due to Nernst diffusion layer is compacted with mean linear flow electrolyte velocity [7].

Table 2. Mass transport correlations in flow-through porous electrodes.

Electrolytic solution	$k_m a = bu^c$			
	Grafito Felt	Reticulated vitreous carbon	Stainless steel fibres	Carbon particles
Ag(I)	————	————	$0.07u^{0.55}$ (a 81 cm ⁻¹ , ϵ 0.907) [7]	$0.0023u^{0.33}$ (particle size 0.11 cm, ϵ 0.33) (this work)
	————	————	$0.12u^{0.95}$ (a 107 cm ⁻¹ , ϵ 0.910) [7]	$0.0029u^{0.50}$ (particle size 0.24 cm, ϵ 0.35) (this work)
	————	————	$0.32u^{0.69}$ (a 193 cm ⁻¹ , ϵ 0.969) [7]	$0.0066u^{0.78}$ (particle size 0.30 cm, ϵ 0.36) (this work)
Cu ²⁺	$3.38u^{0.62}$ [16]	$0.88u^{0.06}$ (100 ppi) [16]	————	————
Hg ²⁺	$3.7u^{0.42}$ [13]	————	————	————
Fe(CN) ₆ ³⁻	$6.0u^{0.36}$ [13]	————	————	————
————	————	$0.002u^{0.08}$ (60 ppi) [19]	————	————

From the correlations $k_m a = bu^c$ showed in the plots, it can be observed that the value of the velocity exponent, c , increases slightly as a function of the particle size, 0.33, 0.50 and 0.78, for 0.11, 0.24 and 0.30 cm, respectively, indicating that the flow pattern is improved as function of the particle size, which is also associated with the increase of porosity, as shown in Table 1. This last is in agreement to that previously reported in a previous paper [7]. On the other hand, the values of the coefficient b , associated with the electrode geometry, increased with the particle size showing the dependence of the mass transport correlation with this parameter.

In Table 2, the mass transport correlations for carbon particles, obtained in this work, were compared to that reported in the literature. It is important to point out that the correlations obtained by Delanghe et al. [13] were obtained in two electrolytic solutions, with an electrode of graphite felt with thickness of 0.9 cm, the former during the deposition of mercury, and the latter during the soluble reduction of $\text{Fe}(\text{CN})_6^{3+}/\text{Fe}(\text{CN})_6^{2+}$; while Nava et al. [16] used graphite felt with thickness of 1.2 cm during the Process $\text{Cu}(\text{II})/\text{Cu}$. From the analysis of these three correlations and the obtained herein, it is clearly observed that the nature of reduction reaction and the shape of the electrode modify the mass transport correlation. Mass transport correlations obtained in reticulated vitreous carbon reported by Nava et al. [16] and Walsh [19] were compared to that reported herein (Table 2); these data indicated that the nature of reduction reaction, electrode material and the shape of the electrode modify the mass transport correlation.

In Table 2 is also shown three correlations performed on stainless steel, with different specific area and porosity, in the same electrolyte to that studied herein [7]. The value b in stainless steel and carbon particles increases as a function of the electrode porosity and magnitude of the electrode. The values of coefficient b for carbon particles were slower in two magnitude order than the obtained on carbon steel electrodes. The b values differences are due to the shape of the electrode, porosity and electrode material. It is important to remark that stainless steel is electrically conductive material ($3.7 \times 10^3 \Omega^{-1} \text{cm}^{-1}$) in contrast to carbon particles ($\sim 25 \Omega^{-1} \text{cm}^{-1}$), which is in the barrier of semiconductors. The value of the exponent c is different in correlations obtained on stainless steel and carbon particles; such slightly variations indicates that the flow pattern is a complex function of the electrode porosity and shape of the electrode material [13, 16, 20]. It is important to mention that correlation of the type $k_m a = bu^c$ for carbon particles are rather limited in the literature. From the analysis of the correlations between stainless steel and carbon based electrodes, it is clearly observed that the electrode material, shape of the electrode, and porosity modify the mass transport correlation.

The comparison of mass transport correlations showed in Table 2 supports that in flow-through porous electrode the best correlation is the obtained through experimental data, because it depends on the electrode material (used as electrode), shape and porosity of the electrode, and the nature of the electrochemical reaction.

The experimental measurements of the potential distribution were carried out during the electrolysis of $\text{Ag}(\text{I})$ ions in the flow-through reactor in a single pass mode of operation (Figure 1). The electrolysis were performed by applying a potential on the current collector, at $z = 0$, $\varphi(z=0) = 0.7 \text{ V}$ vs. SHE, situated at the inlet of the packed bed electrode reactor; and the potential along the porous electrode, $\varphi(z)$, was recorded.

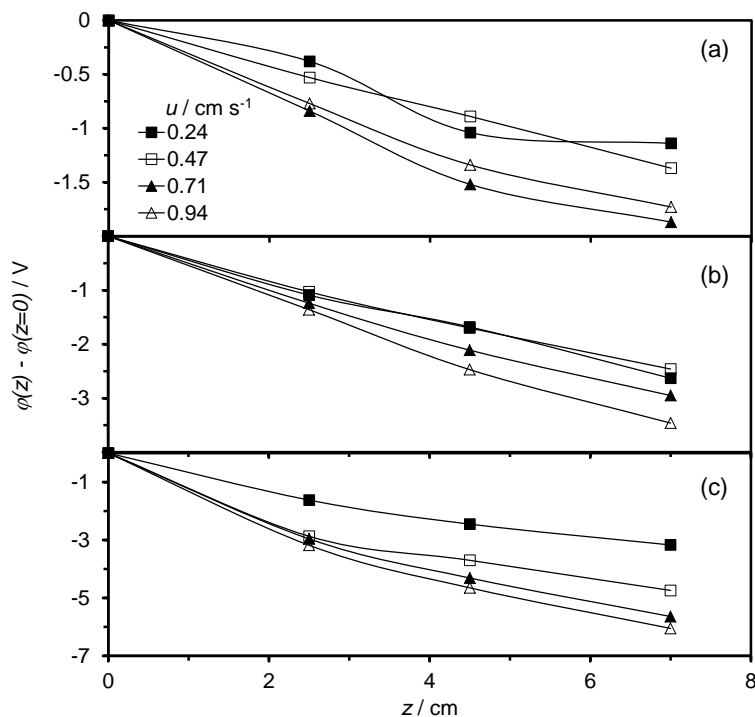


Figure 4. Experimental potential distribution in the flow-through porous electrode reactor during the deposition of Ag(I) ions. Electrolysis potential $\varphi(z=0) = -0.7$ V vs. SHE. Carbon particle sizes: (a) 0.11, (b) 0.24 and (c) 0.30 cm. Mean linear flow electrolyte velocities are showed inside the Figure.

Figure 4 shows the experimental potential distribution, $\varphi(z) - \varphi(z=0)$, at several mean linear velocities for different carbon particle sizes: (a) 0.11, (b) 0.24 and (c) 0.30 cm, respectively. This Figure shows that the electrode potential drop becomes more negative as z increases owing to the concentration decay of the electroactive species [1, 7, 16, 18, 21]. Moreover, the potential becomes more negative as a function of carbon particle size and electrode porosity.

From the analysis of Figure 4(a)-(b) it is observed that the potential distribution did not show systematically depletion with u . However, the potential drop trends to increase as a function of u in the set of electrolysis shown in Figure 4(c). The potential distribution obtained herein was fitted with a model provided in literature [7, 21], which neglects potential distribution in the electrode material; however, the experimental data reported here did not fit with those obtained theoretically. This last is attributed to the potential distribution in the carbon material. A potential distribution model that includes such potential distribution in the material should help for this analysis; however it was beyond of the scope of this paper.

It is important to point out that the maximum potential drop before hydrogen evolution starts will be: $\varphi(z) - \varphi(z=0) = -1.7 - (-0.7) = -1$ V. This allows a potential window of 1 V between the deposition of Ag(I) ions and the beginning of the hydrogen evolution reaction. This criterion was partially satisfied in the flow-through electrode with carbon particles of 0.11 cm, at u of 0.24 and 0.47 cm s^{-1} . For design purposes, the hydrogen evolution should be preferably avoided, with carbon particles of 0.11 cm, adjusting the values of the mean linear flow velocity and the electrode length.

5. CONCLUSIONS

This paper deals with the experimental mass transport characterization ($k_m a = bu^c$) and potential distribution during the deposition of silver ions on carbon particles of three different sizes used as flow-through porous electrode.

The experimental mass transport characterization showed that for 0.11 cm of particle size, the value of the coefficient b , associated with magnitude of porous electrode, is 0.0023, while for 0.24 and 0.30 cm are 0.0029 and 0.0066, respectively. On the other hand, c values for 0.11 cm is 0.33, while for 0.24 and 0.30 cm are 0.50 and 0.78, indicating that the flow pattern is a complex function of the shape of the electrode.

The comparison of mass transport correlations, with other reported in the literature, suggests that the best correlation is the obtained through experimental data owing to it depends on the electrode material (used as electrode), shape and porosity of the electrode, and the nature of the new metallic phase.

The experimental electrode potential distribution becomes more negative as a function of the axial length of the electrode, and carbon particle size and porosity. However, the electrode potential distribution in the flow-through porous electrode presented potential distribution on the electrode matrix of carbon particles. For design purposes, the hydrogen evolution should be preferably avoided, with carbon particles of 0.11 cm, adjusting the values of the mean linear flow velocity and the electrode length.

ACKNOWLEDGMENTS

The authors are grateful to CONACYT and UASLP for the founding via the project FORDECYT No. 190966.

References

1. D.N. Bennion, J. Newman, *J. Appl. Electrochem.*, 2 (1972) 113.
2. T. Doherty, J. G. Sunderland, E. P. L. Roberts, D. J. Pickett, *Electrochim. Acta*, 41 (1996) 519.
3. M.S. El-Deab, M. M. Saleh, B. E. El-Anoduli, B. G. Ateya, *J. Electrochem. Soc.*, 146 (1999) 208.
4. A. Gaunand, D. Hutin, F. Coeuret, *Electrochim. Acta*, 22 (1977) 93.
5. M. R. V. Lanza, R. Bertazzoli, *J. Appl. Electrochem.*, 30 (2000) 61.
6. M. J. Matloz, J. Newman, *J. Electrochem. Soc.*, 133 (1986) 1850.
7. J. L. Nava, M. T. Oropeza, C. Ponce de León, J. González-García, A. J. Frías-Ferrer, *Hydrometallurgy*, 91 (2008) 98.
8. E. J. Podlaha, J. M. Fenton, *J. Appl. Electrochem.*, 25 (1995) 299.
9. C. Ponce de León, D. Pletcher, *Electrochim. Acta*, 41 (1996) 533.
10. M. M. Saleh, *J. Phys. Chem. B*, 108 (2004) 13419.
11. E. A. Soltan, S. A. Nosier, A. Y. Salem, I. A. S. Mansour, G. H. Sedahmed, *Chem. Eng. J.*, 91 (2003) 33.
12. J. M. Trainham, J. Newman, *J. Electrochem. Soc.*, 124 (1977) 1528.
13. B. Delanghe, S. Tellier, M. Astruc, *Electrochim. Acta*, 35 (1990) 1369.
14. A. Ratel, G. Lacoste, *J. Appl. Electrochem.*, 12 (1982) 267.
15. R. Alkire, B. Gracon, *J. Electrochem. Soc.*, 122 (1975) 1594.

16. J. L. Nava, A. Recéndiz, L. G. González, G. Carreño, F. Martínez, *Potugaliae Electrochim. Acta*, 27 (2009) 381.
17. J. M. Marracino, F. Coueret, S. Langlois, *Electrochim. Acta*, 32 (1987) 1303.
18. T. Z. Fahidy, *Principles of Electrochemical Reactors Analysis*, Elsevier, (1985).
19. F. C. Walsh, *A First Course in Electrochemical Engineering*, Electrochemical Consultancy, (1993).
20. S. Langlois, F. Coeuret, *J. Appl. Electrochem.*, 19 (1989) 51.
21. R. E. Sioda, *Electrochim. Acta*, 16 (1971) 1569.

© 2013 by ESG (www.electrochemsci.org)